Indian Journal of Chemical Technology
Vol. 31, March 2024, pp. 175-185
DOI: 10.56042/ijct.v31i2.5981

# A comparative photocatalytic degradation study of Thymol blue dye over pristine ZnO and Er-doped ZnO

Yogeshwar Digambar Kaldante[1]*, Ramesh Natha Shirsat[1]& Manohar Ganpat Chaskar[2]

[1]Department of Chemistry, PDEA's Annasaheb Waghire College, Otur, Pune, Maharashtra – 412 409, India

[2]Department of Chemistry, PDEA's Prof. Ramkrishna More College, Akurdi, Maharashtra – 411 044, India

*E-mail: ydkaldante@gmail.com (YDK), chaskarmanohar@gmail.com (MGC)

*Received 5 October 2023; accepted 12 February 2024*

Existing work describes the synthesis of pristine ZnO and Er-doped ZnO by mechanochemical method and evaluation of the photocatalytic activity synthesized samples towards photochemical degradation of Thymol Blue dye. The right calcination temperature has been gained from TGA-DTA analysis. FTIR results show the formation metal oxides from their respective precursors upon calcinations. XRD data obtained for ZnO and Er-ZnO clearly suggest the hexagonal wurtzite crystallite structures. FE-SEM images established nanocrystalline morphology. The elemental pureness of these samples is confirmed by EDX study. The optical band gaps are determined from UV-Visible spectroscopic studies. PL spectra are used to explore the additional information about optical properties of said photocatalysts. The comparative studies of photocatalytic activities of these materials towards degradation of Thymol Blue dye is carried out with respect to involved operational parameters. The possible degradation intermediates and products are also illustrated with HPLC & HRMS techniques.

**Keywords:** Er doped ZnO, Photocatalytic degradation**,** PCD efficiency, Thymol Blue, ZnO

## Introduction

Metal oxide catalysis is one of the most important fields studied from 1950's as it deals with most of the industrially applicable chemical processes and catalyst families[1]. Metal oxide constitutes very huge catalyst family includes clays, alumina, silica, zeolites, ZnO, $TiO_2$, $ZrO_2$, porous and mesoporous oxides, polyoxometallates, multicomponent mixed oxides, perovskites, hexaaluminates, etc.[1]. These mentioned catalytic materials have wide applications in the industrially valuable chemical process such as acid-base catalysis[2, 3], selective oxidation reactions[4, 5], total oxidation reactions[6, 7], biomass transformation reactions[8-10], photocatalysis[11-13], etc. Among the mentioned process photocatalysis is relatively young but more interesting field of research. Research in the field of heterogeneous photocatalysis from the last two to three decades established it as an effective solution for the environmental remediation[14].

The water pollution is one of the severe problems of the present days all over the world. The conventional methods including physical, chemical and biological processes are not sufficient to get rid of this problem of water pollution. Due to some advantages over these conventional methods of water treatment heterogeneous photocatalysis has been established as a promising alternative for the detoxification of industrial effluents[15, 16] and environmental protection[16]. Heterogeneous photocatalysis is capable of total mineralization of organic pollutants[17]. Various metal oxides have been well utilized and are nontoxic, stable, highly photosensitive, wide band gap heterogeneous photocatalyst materials. Appropriate positioning of conduction band and valence band makes the semiconductor metal oxides to absorb the light and show photocatalytic activity. Solar light activated semiconductor metal oxide like ZnO; $TiO_2$ usually promotes the photodegradation of water pollutants[18]. Typically solar or artificial light activated semiconductor metal oxide catalysts undergo electron-hole pair generation. These electron-hole pair further in situ generates highly energetic hydroxyl and superoxide radicals which are capable of non-selective complete breakdown of the pollutants[19]. Organic pollutants generated by various industries like drug and pharmaceuticals[20], herbicides[21], pesticides[22], dyes[23], etc. have been extensively elaborated by the researchers. Among aforesaid organic pollutants synthetic dyes are one of the water contaminants which severely damage the quality of water. Dyes are very extensively employed in the

various industries like paper, plastic, leather, rubber, paint, textiles, etc. for colouring purpose. Hence, wastewater from these industries is enriching with large amount of dyes which can causes severe health related disorders and diseases[24, 25].The removal or degradation of such harmful dyes is necessary for good quality of water which can be achieve by means of heterogeneous photocatalysis.

Among the several metal oxides ZnO is found to be the most suitable candidate for the visible light mediated photocatalysis. The catalytic activity of ZnO can be well enhanced by the doping of pristine ZnO with metal[26] or non-metal[27]. Doping of ZnO with rare earth metal enhances its photocatalytic activity to the greater extent[28]. Some examples of doping of rare earth metal to zinc oxide for its enhanced photocatalytic activity is available in the literature. Present study highlights comparative studies of photocatalytic activity of pristine ZnO and Er doped ZnO obtained by mechanochemical method with reference to the Thymol blue (Fig. 1) as a model dye pollutant and operational parameters like dye concentration, photocatalyst loading capacity, pH of dye solution, irradiation time, etc. The possible degradation intermediates and products were also illustrated with HPLC & HRMS techniques furthermore the possible mechanism of photocatalytic dye degradation is also proposed.

## Experimental Section

### Material

$Zn(CH_3COO)_2.2H_2O$ (assay 99.5%), $Er(CH_3COO)_3.4H_2O$ (assay 99.0 %), $H_2C_2O_4.2H_2O$ (assay 99.0%), Thymol blue dye (assay 99.0%) and other needed chemicals used during this work were AR grade reagents obtained from S.D. Fine Chemicals, India and used as received. All the experimental solutions were prepared in double distilled water. The pH of these solutions was adjusted to required values with dil. NaOH and dil. HCl wherever necessary.

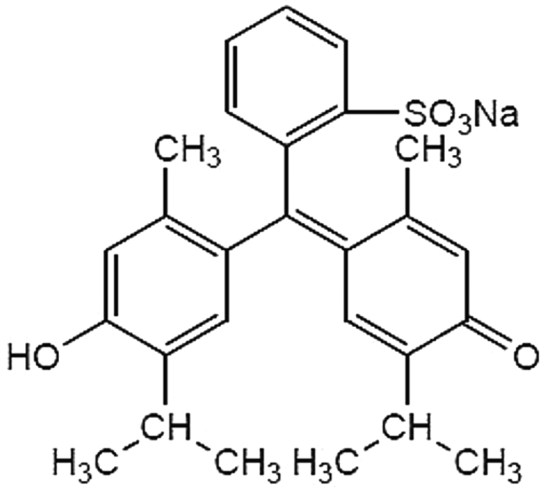


Fig. 1 — Structure of the Thymol blue dye

### Synthesis of photocatalyst

Two step processes was adopted for the synthesis of Er-doped ZnO catalyst. Therein, the synthesis of erbium zinc oxalate dihydrate precursor followed by its thermal decomposition is involved. In the first step 0.925 M zinc acetate dihydrate and 1.20 M oxalic acid dihydrate was hand grinded till paste of zinc oxalate dihydrate is formed. To this 0.075 M Erbium acetate tetrahydrate was added and the hand grinding is continued in agate mortar with pestle for 25 min at room temperature under subsequent drying under IR lamp for getting erbium zinc oxalate dihydrate precursor. In next step the erbium zinc oxalate dihydrate precursor was calcined at 500℃ to yield Er-doped ZnO powder. Pristine ZnO was obtained as per method described in our previous article[29] and with calcination at 500℃ and was used for the comparative study.

### Equipments

The transformation temperature of erbium zinc oxalate dihydrate precursor to the Er-doped ZnO was gained by thermogravimetric analysis instrument (Shimadzu, TG - DTG - 60H) and FT-IR (*PerkinElmer* UATR Spectra Two) spectrometer.For Er-ZnO and ZnO crystallites the X-ray diffraction (XRD) pattern was obtained withXRD instrument (*RikaguMiniflex*-600) having Cu Kα radiation (λ = 1.5418Å) source and the average crystallite size (D) of the particles was determine from the well-known Debye-Scherrer equation[30]:

$$D = \frac{0.90\times\lambda}{\beta\times cos\theta} \quad \ldots (1)$$

The morphological characterization of pure and doped ZnO was done with FE-SEM instrument (JEOL JSM-6360A). The elemental composition and purity of the synthesized materials was deliberate with energy dispersive X-ray (EDX) spectra. The optical band gaps of pristine ZnO and Er doped ZnO were estimated from spectra obtained with UV-visible Spectrophotometer (Perkin Elmer Lambda 365). The

optical properties of mentioned photocatalysts was further studied with room temperature PL spectra recorded with spectrofluorometer Shimadzu, RF-5301PC over 200 – 800 nm range with excitation wavelength 320 nm. The photocatalytic reactions were carried out at room temperature in batch reactor under solar light. Absorbance measurement with digital colorimeter (EQUIP-TRONICS EQ-353) is used forbthe estimation of degradation efficiency. The initial pH of suspension was adjusted by aid of pH meter (LABTRONICS LT-11).Light intensity was at times checked by LUX meter.The possible mechanism of photocatalytic dye degradation and intermediates involved therein is also investigated with the help of HPLC – HRMS (Brucker Compass Impact HD) technique.

**Photocatalytic degradation experiments**

Entirely photocatalytic reactions were performed in batch reactor constituted with cylindrical glass vessel (100 mL capacity) covered with glass cool trap and mounted on magnetic stirrer. A known quantity (50, 75, 100, 125, 150, 175 and 200 mg) of photocatalyst was added in Thymol blue dye (100 mL) solution in water. This mixture was then agitated to get uniform suspension by means of ultra-sonication for 5 min. Initial pH of suspension was recorded. Entire setup was then kept under sunlight irradiation with constant stirring for specific period of time between 10:00 a.m. and 4:00 p.m. The extent of photochemical degradation or degradation efficiency at an interval of 1 h was primarily monitored with colorimetric absorbance measurement at predetermined $\lambda_{max}$ value of dye and the percent of degradation (%D) was calculated using following formula.

$$\% D = \frac{100\times[A_0 - A_t]}{[A_0]} \quad \ldots (2)$$

where %D is percent degradation, $A_0$ is initial absorbance and $A_t$ is absorbance at time *t*.

## Result and Discussion

**Characterization of Pure ZnO and Er-doped ZnO**

The process of conversion of metal (Zn and Er-Zn) oxalate dihydrate precursors to corresponding oxides (ZnO and Er-doped ZnO) was studied by TGA-DTA analysis and FT-IR spectroscopy, The photocatalysts gained was further characterized by XRD, FE-SEM and EDX study. The optical properties of these photocatalysts were studied with UV-visible and PL spectroscopy.

***Thermal gravimetric analysis***

Fig. 2 shows the TGA-DTA plots for metal (Zn and Er-Zn) oxalate dihydrate precursors. From the DTA plots it is clear that thermal decomposition of mentioned metal oxalate dihydrate precursors occurred with two sharp endothermal steps from 25℃ to 450 ℃ to give ZnO and Er-ZnO. The first sharp endotherm in the both DTA curves represents loss of two water molecules (theoretical weight loss 19%).The second sharp endotherm in the both DTA represents loss of oxalate moiety (theoretical weight loss 38%). In case of both the precursors the observed weight losses in the TG curves fairly matches with theoretical weight losses. The conversion temperature for metal (Er-Zn and Zn) oxalate dihydrate precursors to ZnO and Er-ZnO is 430 – 450 ℃. In the present studies 500 ℃ is consider as suitable calcination temperature.

***FT-IR spectroscopic study***

Fig. 3 shows changes in the FT-IR spectra during the transformation of metal (Zn and Er-Zn) oxalate dihydrate precursors to pure ZnO and Er-ZnO. The FTIR spectra of metal (Zn and Er-Zn) oxalate dihydrate precursors consist of bands (as tagged in the Figs) corresponding to various symmetric and asymmetric stretching and bending vibrations related to bondings present in the precursors. Diminishing of all these bands other than that centered at 450 $cm^{-1}$

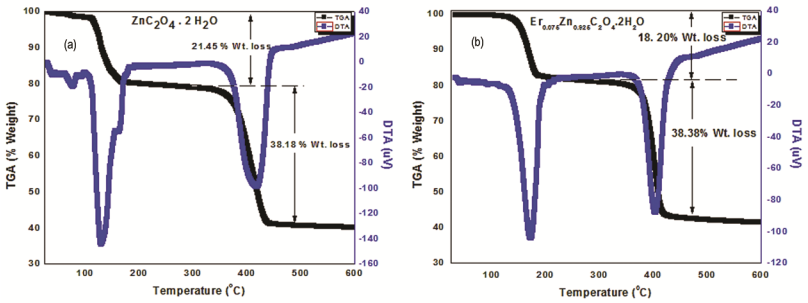


Fig. 2 — TG-DTA plots for zinc oxalates dihydrate and erbium zinc oxalates dehydrate

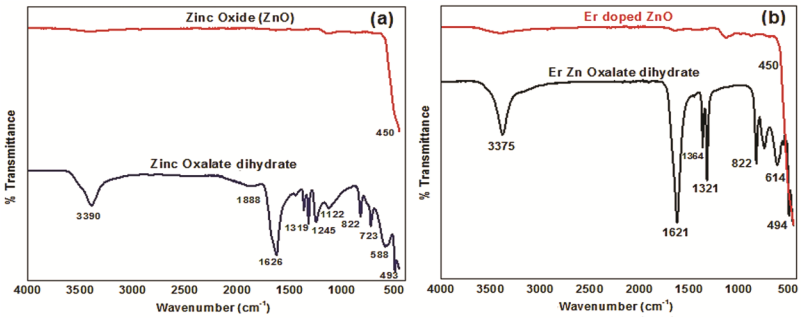


Fig. 3 — Changes in FT-IR spectra during the transformation of oxalates to oxides

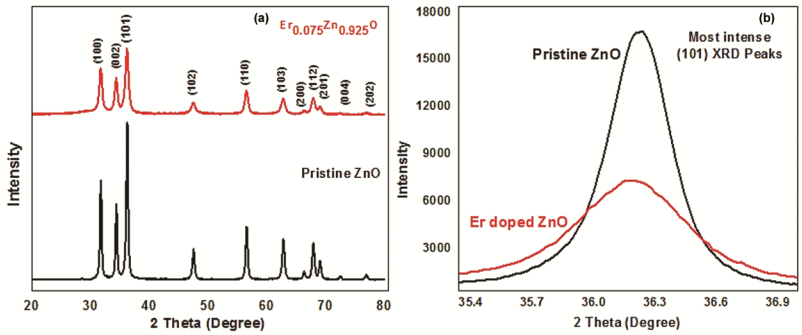


Fig. 4 — XRD patterns of (a) in the full range and (b) slow scans of corresponding XRD patterns in 2θ range of 35.4 to 36.9° for pristine ZnO and Er-doped ZnO powders

upon calcination of these precursors at 500 °C confirms the formation of pure ZnO and Er-ZnO and same was also confirmed by XRD study.

***X-Ray diffraction (XRD) study***

The Fig. 4a shows the XRD patterns of ZnO and Er-ZnO powder. Data mentioned series of peaks centered at 2θ = 31.74°, 34.38°, 36.22°, 47.50°, 56.58°, 62.84°, 66.36°, 67.92°, 69.18°, 72.66°, 76.88° for pure ZnO and at 2θ = 31.68°, 34.34°, 36.16°, 47.48°, 56.56°, 62.82°, 66.26°, 67.90°, 69.14°, 72.64°, 76.86° for Er-ZnO powder. These data finely agreed as per JCPDS card number 36-1451[31].The peaks are indexed to (100), (002), (101), (102), (110), (103), (200), (112), (201), (004) and (202) planes of wurtzite structure of ZnO respectively. Lowering of XRD peak intensity (peak broadening) and slight shift in the Bragg angles (2θ) to lower values in case of Er-doped ZnO than that of pure ZnO is due to substitution of Er at Zn sites in the crystal. Absence of any additional peak in the XRD pattern of Er doped ZnO clearly reflect that erbium oxide or any other phase of erbium is not formed & elemental Er is also absent in the sample which also supports that the Er is doped at the site of Zn in the ZnO crystal lattice. That is there is no formation of composite material. The Fig. 4b shows slow scan of (101) reflections of corresponding XRD pattern (shown in Fig. 4a) in 2θ range of 35.4 to 36.9°. These slow scans are used to find average crystallite size of pure ZnO and Er- doped ZnO by using Debye-Scherer relation[30].

The average crystallite size gained for ZnO and Er-doped ZnO and are 20 ± 0.5 nm and 11 ± 0.5 nm, respectively. The lattice strains calculated by using tangent formula[32] was found to be 0.29 ± 0.004 and 0.53 ± 0.002, and the specific surface areas determined by using Sauter Formula[33]was found to be 52 ± 0.10 $m^2$ / g and 94 ± 0.20 $m^2$ / g for pure ZnO and Er- doped ZnO, respectively. Due to small particle size of Er-ZnO than that of ZnO the average surface area is found to be more in case of Er-ZnO and this may be one of the reasons for the enhancement of photochemical degradation activity of Er doped ZnO sample than that of bare ZnO.

***FE-SEM study***

The morphological characterization of ZnO and Er doped ZnO was studied by using field emission scanning electron microscopy (FESEM). Fig. 5 indicates the FESEM photographs of ZnO and Er doped ZnO powders. The FESEM image of pure ZnO shows formation of nearly homogeneous phase

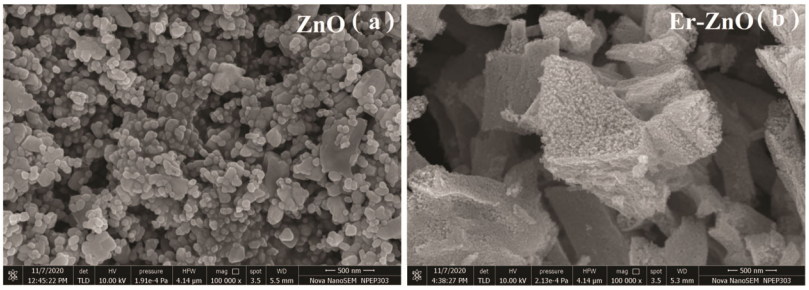


Fig. 5 — FESEM photographs of (a) pristine ZnO and (b)Er-doped ZnO

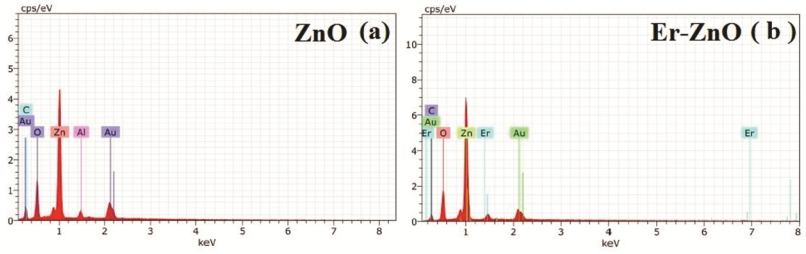


Fig. 6 — EDX spectra of (a) pristine ZnO and (b) Er-doped ZnO

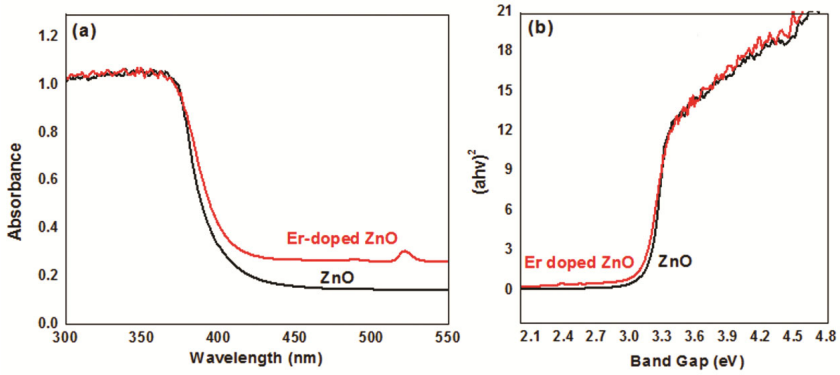


Fig. 7 — (a) UV-visible spectra and (b) Tauc plots of pristine ZnO and Er-doped ZnO

having non-agglomerated, dense particles of hexagonal morphology whereas the FE-SEM image of Er-doped ZnO indicates the formation of particles having sponge like morphology. The mean particle size is found be around 68 nm and 22 nm, respectively, for pure ZnO and Er-doped ZnO.

***EDX analysis***

Energy Dispersive X-ray (EDX) spectra of pure ZnO and Er-doped ZnO is shown in Fig. 6. Fig. 6a indicates peaks corresponding to Zn and O only in significance with purity of the zinc oxide. Fig. 6b indicates peaks corresponding to Er, Zn and O only representing elemental purity of sample. The additional peaks corresponding Au, Al and C is due to their use for the preparation of conducting film to record the EDX spectra.

***UV-Visible Spectra***

Fig. 7a represents UV-visible spectra of pure ZnO and Er doped ZnO having clearly located optical extinction bands in the range of 370 nm to 415 nm, respectively. The band gap energy obtained for pure ZnO and Er-doped ZnO was found to be 3.164 eV and 3.095 eV, respectively, using UV-visible spectra and Tauc plots (Fig. 7b).

***Photoluminescence spectra***

Fig. 8 represents room temperature PL spectra recorded over 350 – 650 nm range with excitation wavelength 320 nm. PL spectra of both samples shows weak but clear UV emission peak maxima fixed near 383 nm as contribution of excitonic recombination matching with NBE emission of ZnO[34, 35]. These samples shows strong emission band centered at 500 – 510 nm related to

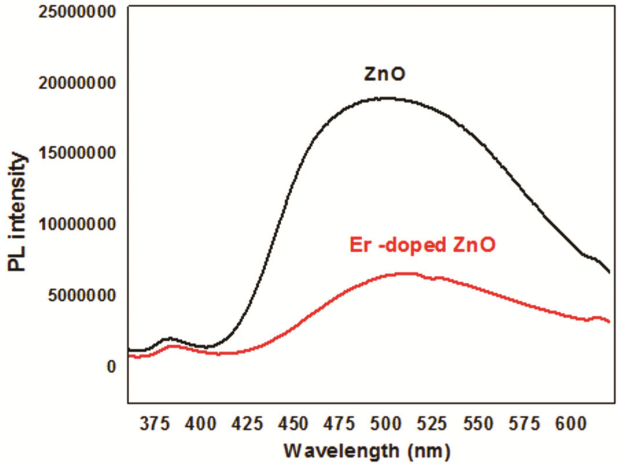


Fig. 8 — Room temperature PL spectra of pristine ZnO and Er-doped ZnO

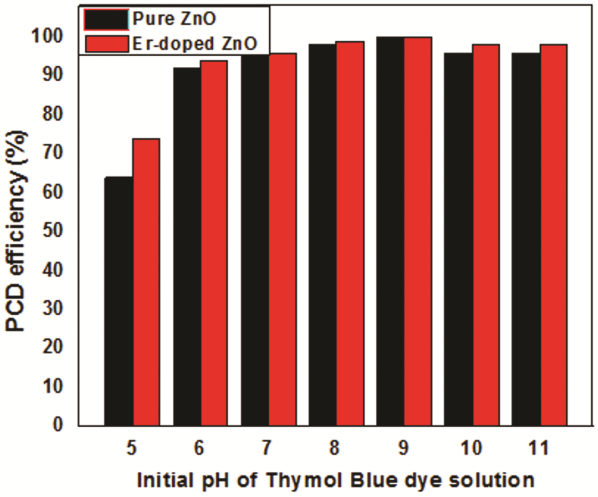


Fig. 9 — Effect of initial pH of Thymol blue dye solution on photocatlytic degradation efficiency

the green emission attributed to the singly ionized oxygen vacancy in ZnO sample and the emission results from the radiative recombination of a photogenerated hole with an electron occupying the oxygen vacancy[36]. Er- doped ZnO have lower PL intensity peaks than that of pure ZnO which is in accordance to slower recombination of photogenerated hole-electron pairs[37] and hence accounted for the improved optical properties of Er- doped ZnO than that of ZnO.

**Photocatalytic activity of pristine ZnO and Er-doped ZnO catalysts**

Photocatalytic activities of pristine ZnO and Er-doped ZnO were investigated with reference to the operating factors such as initial dye concentration, photocatalyst loading capacity, pH of dye solution, irradiation time, etc.

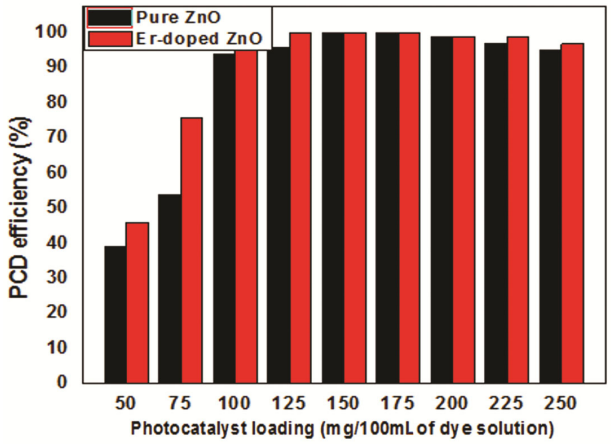


Fig. 10 — Effect of ZnO and Er-ZnO loading on photocatlytic degradation efficiency

***Effect of the initial pH of Thymol Blue dye solution***

Photocatalytic degradation of Thymol blue dye of randomly chosen concentration of 50 ppm over pure ZnO and Er-doped ZnO was measured at altered pH from 5 to 11 with 150 mg of photocatalyst / 100mL of dye solution and with 6 h of sunlight irradiation (Fig. 9). The pH of the suspensions only pre-adjusted prior to irradiation and not considered within the course of reaction.

In accordance with well established point the photocatalytic degradation of Thymol blue dye at pH 5 and 6 was found to be less because of slight (<1%) dissolution of the ZnO and Er-doped ZnO in acidic medium[38]. The extent of degradation of Thymol blue was observed to increase with the increase in initial pH of suspensions. In alkaline medium, excess of hydroxyl anions stimulates photo-generation of hydroxyl radicals which are main oxidizing species in the degradation process[39]. Hence, degradation efficiencies of ZnO and Er-doped ZnO were found to be greater at alkaline pH (9-11). At pH 9, the efficiency was highest for both photocatalysts.

***Effect of the loading of ZnO and Er-doped ZnO***

Degradation of Thymol blue of randomly chosen concentration of 50 ppm of over ZnO and Er-doped ZnO was studied at variable loading quantity of ZnO and Er-doped ZnO from 50 mg-250 mg/100 mL of dye solution at best pH=9 and with 6 h of sunlight irradiation (Fig. 10). In case of ZnO, the degradation efficiency was gradually improved up to loading amount of 200 mg/100 mL of dye solution, whereas in case of Er-doped ZnO the efficiency was found to increase up to loading amount of 150 mg/100 mL of dye solution. In case of both the photocatalysts loading more than 175 mg/100 mL of dye solution

results in the formation of more turbid solutions and hence causes screening and shadowing effect of light so the degradation efficiency was found to be slightly decreased. Hence, 125 mg of Er-doped ZnO /100 mL (50 ppm) of dye solution are sufficient for the complete degradation of Thymol blue within 6 h of irradiation and this quantity is less than that of pure ZnO. Because of smaller particle size of Er-doped ZnO than pure ZnO, it provides more surface area for the adsorption of dye molecules and their degradation.

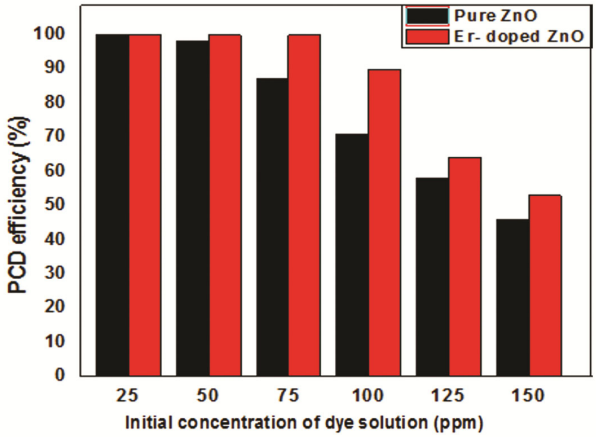


Fig. 11 — Effect of the initial concentration of dye solution on degradation efficiency

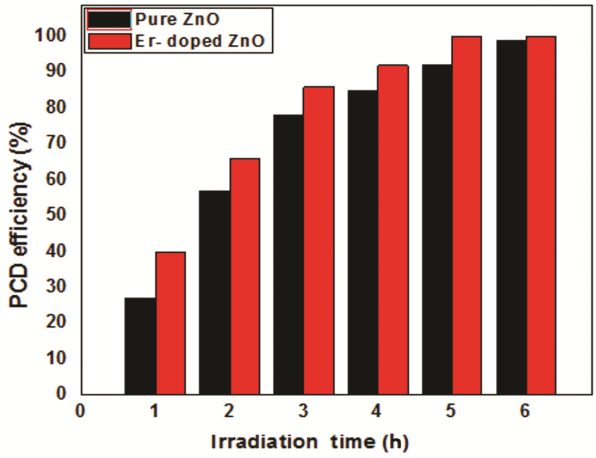


Fig. 12 — Effect of irradiation time on degradation efficiency

***Effect of the initial concentration of the dye solution***

The degradation efficiency of Thymol Blue over ZnO and Er-doped ZnO at various initial concentrations in the range 25- 150 ppm was studied with respect to sunlight irradiation time at the best pH 9 of the suspension. The efficiency is measured in terms of decrease in the absorbance (increase in % degradation) of Thymol blue and results are showed in Fig. 11. Each of the 25, 50 and 75 ppm of Thymol blue was completely degraded over 150 mg Er-doped ZnO /100 mL of the solution and it shows more degradation efficiency than pure ZnO. As expected the efficiency was found to be declined with increase in concentration of dye solutions because of the formation of intense coloured and turbid solution and thereby preventing the photons to reach the photocatalyst surface and its activation.

***Effect of irradiation time***

The PCD efficiency of ZnO and Er-doped ZnO in sunlight gradually increases with increase in irradiation time (Fig. 12). 100 mL of 50 ppm Thymol blue solution was completely mineralized over 150 mg Er-doped ZnO at the pH 9 upon 5 h of sunlight irradiation whereas for identical experiment with ZnO the time required for the almost complete (98%) photocatlytic degradation was found to be 6 h.

Fig. 13 indicates the UV-visible spectra reflecting photocatalytic degradation of Thymol blue with

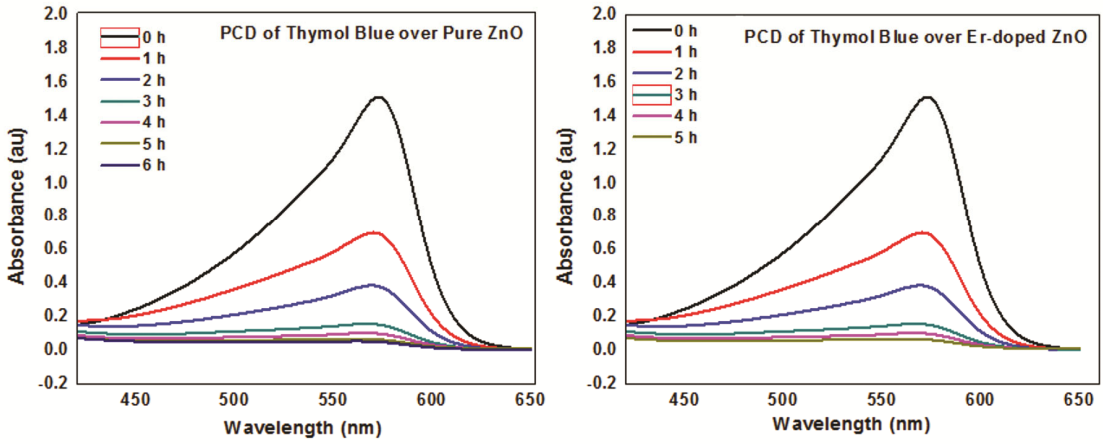


Fig. 13 — UV-Visible spectra for PCD of Thymol blue dye over (a) pristine ZnO and (b) Er-doped ZnO

Table:1 — Reusability of ZnO and Er doped ZnO photocatalysts

| Photocatalyst | Photocatalytic degradation efficiency (Percent degradation of Thymol blue) | | |
|---|---|---|---|
| | Cycle 1 | Cycle 2 | Cycle 3 |
| Pristine ZnO | 92 | 88 | 83 |
| Er-doped ZnO | 100 | 94 | 91 |

Experimental conditions (optimized) = 100 mL, 50 ppm Thymol blue dye,150 mg catalyst, pH 9 and irradiation time 5 h

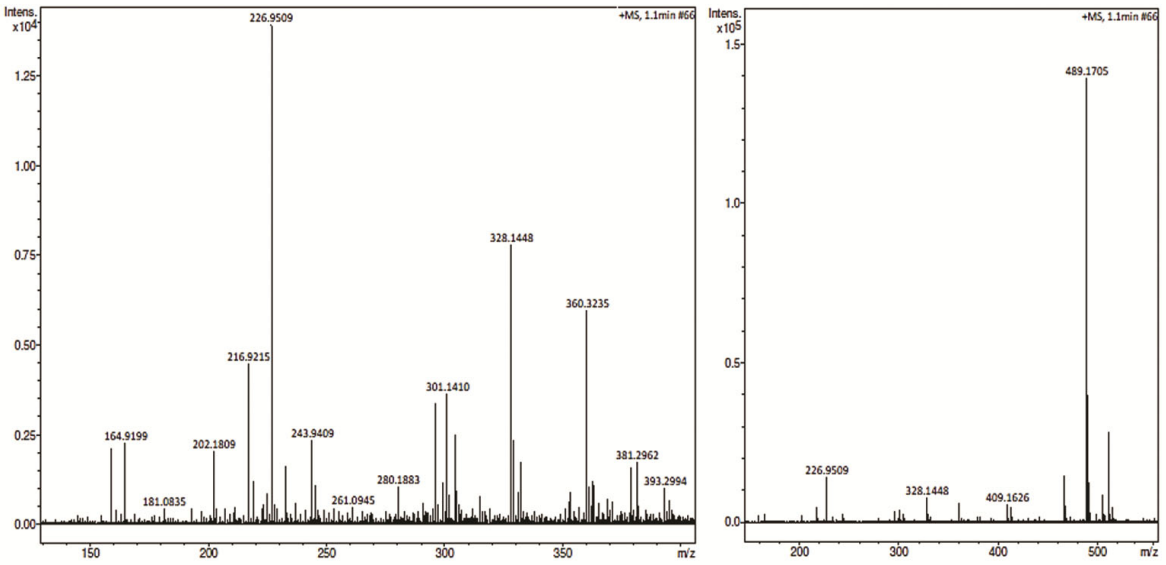


Fig. 14 — HPLC-HRMS (LCMS) spectra of Thymol blue dye solution from the course of reaction

irradiation time. The absorbance of dye solution goes on decreasing with increase in irradiation time. In case of photocatalytic degradation of dye over Er-doped ZnO photocatalyst the absorbance nearly becomes zero within 5 h of irradiation (Fig. 13b), whereas for the same in case of pure ZnO requires 6 h (Fig. 13a). The PCD efficiency was directly proportional to the irradiation time. Mechano-chemically synthesized Er-doped ZnO is found to be better photocatalysts in sunlight than pure ZnO.

***Reusability of ZnO and Er doped ZnO photocatalysts***

The stability of pristine ZnO and Er-ZnO catalysts were also studied. These materials were recovered from reaction mixture by centrifugation followed by filtration, washing, drying for activation and were reused 2 times under identical (optimized) experimental conditions. It is found that even reused catalysts were efficient for the Thymol blue dye degradation without large change in its photocatalytic activity. The data obtained for the reusability of ZnO and Er doped ZnO photocatalysts is mentioned in the Table 1. Here cycle 1 stands for original or first time use of said catalysts and so on.

**Possible Degradation Mechanism and Degradation Products**

The degradation products were investigated with HPLC - HRMS (LCMS) data obtained using Brucker Compass Impact HD instrument and the possible dye degradation mechanism was also illustrated. During the degradation process, adsorption of organic dye molecules on the surface of excited ZnO particles activates them due to the reaction with energetic •OH radicals having electrophilic characters and which preferentially attacks on electron rich *ortho* or *para* carbon atoms of dye molecule. Hence the dye molecule undergoes fragmentation or degradation.

Fig. 14 shows the HPLC-HRMS chromatogram of Thymol blue dye solutions collected during the course of reaction. The possible mechanism of degradation is shown in the Fig. 15 and from the data of HPLC-HRMS (LCMS) analysis of the dye solutions collected during the course of reaction identified the degradation intermediates / fragments and products are given in the Table 2.

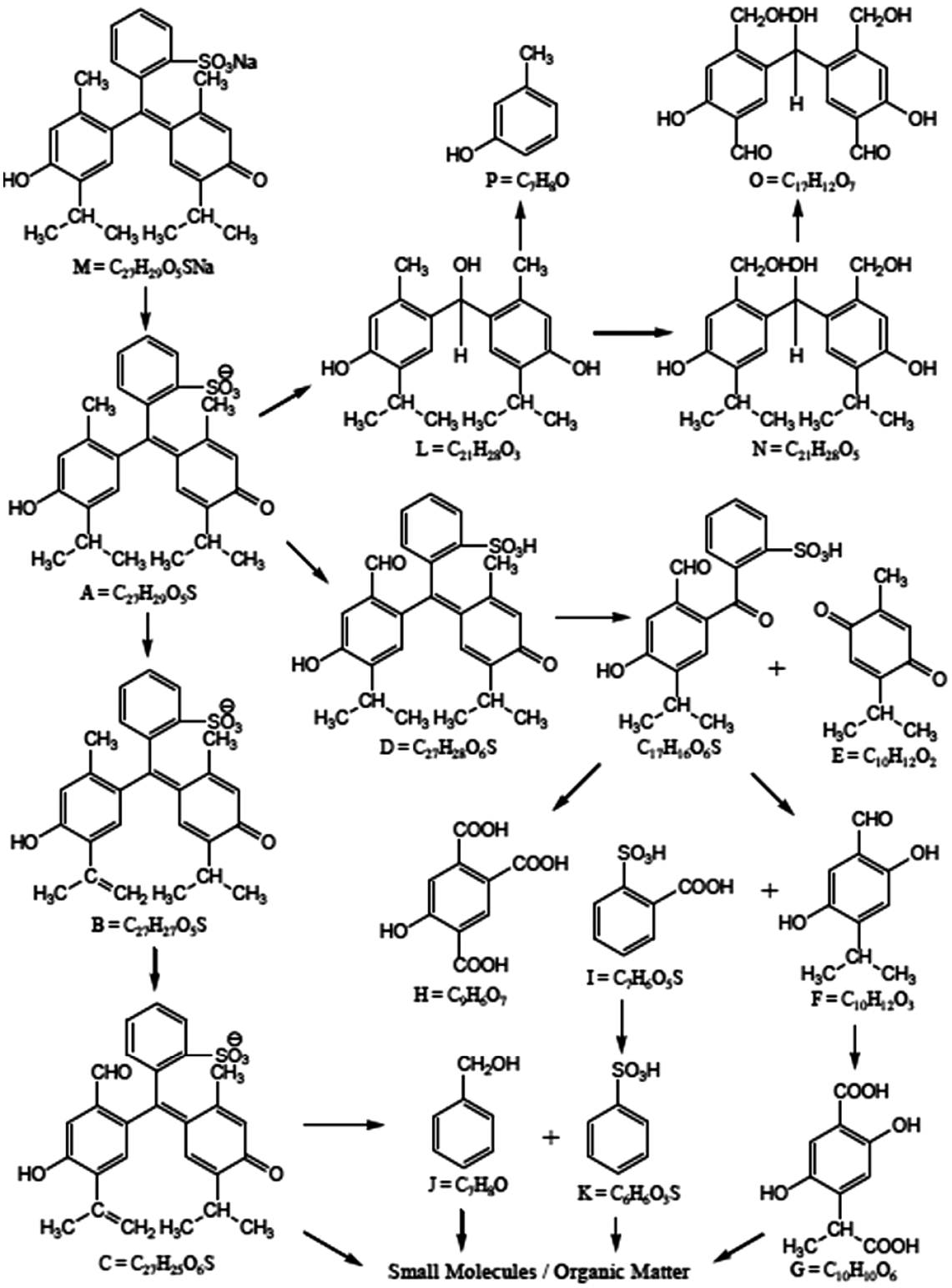


Fig. 15 — Possible mechanism of Thymol Blue dye degradation

Table 2 — Identified photocatalytic degradation intermediates during Thymol blue dye degradation

| Intermediate | Molecular Formula | Molecular Weight |
|---|---|---|
| Thymol Blue (M) | $C_{27}H_{29}O_5SNa$ | 489.17 |
| A | $C_{27}H_{29}O_5S$ | 467.18 |
| B | $C_{27}H_{27}O_5S$ | 464.89 |
| C | $C_{27}H_{25}O_6S$ | 478.00 |
| D | $C_{27}H_{28}O_6S$ | 481.00 |
| E | $C_{10}H_{12}O_2$ | 164.91 |
| F | $C_{10}H_{12}O_3$ | 181.08 |
| G | $C_{10}H_{10}O_6$ | 226.95 |
| H | $C_9H_6O_7$ | 226.95 |
| I | $C_7H_6O_5S$ | 202.18 |
| J | $C_7H_8O$ | 107.98 |
| K | $C_6H_6O_3S$ | 158.96 |
| L | $C_{21}H_{28}O_3$ | 328.14 |
| N | $C_{21}H_{28}O_5$ | 360.32 |
| O | $C_{17}H_{12}O_7$ | 328.14 |
| P | $C_7H_8O$ | 107.98 |

## Conclusion

In the present investigation, the pristine ZnO and Er-doped ZnO photocatalysts were synthesised by simple mechanochemical method and characterised by different techniques. The peak broadening and shifting in XRD pattern of Er-doped ZnO as compare to pure ZnO confirmed the insertion of Er into ZnO lattice. 100 mL each of 25, 50 and 75 ppm of Thymol blue dye solutions at pH = 9 were totally mineralized over 150 mg Er-doped ZnO within 3.5, 5 and 6 h of sunlight irradiation, respectively. Er-doped ZnO was verified to be more efficient photocatalyst under sunlight irradiation than pristine ZnO. The more photocatalytic activity of Er-doped ZnO over pure ZnO is may be due to availability of more surface area of nanoparticles as shown by XRD data calculations and improved optical properties like lowering of band gap energy, less or slow electron-hole pair recombination probability, availability of additional electronic states, etc. as mentioned by UV-visible and PL spectroscopic studies. The effect of different operating factors on the degradation of Thymol blue dye was successfully examined. The reusability of ZnO and Er doped ZnO photocatalysts for PCD of the dye is also studied. With the help of HPLC-HRMS technique the different degradation intermediates or products formed is illustrated and the possible mechanism of dye degradation is proposed.

## Acknowledgement

Authors specifically thank to PDEA's Annasaheb Waghire College, Otur and Savitribai Phule Pune University, Pune for offering their continuous and valuable support in all respect.

## References

1 Védrine J C, Heterogeneous catalysis on metal oxides, *Catalysts*, 7 (2017) 341.
2 Ohyama J, Kanao R, Ohira Y & Satsuma A, The effect of heterogeneous acid–base catalysis on conversion of 5-hydroxymethylfurfural into a cyclopentanone derivative, *Green Chem*, 18 (2016) 676.
3 Yan T, Bing W, Xu M, Li Y, Yang Y, Cui G, Yang L & Wei M, Acid–base sites synergistic catalysis over Mg–Zr–Al mixed metal oxide toward synthesis of diethyl carbonate, *RSC Adv*, 8 (2018) 4695.
4 Blasco T & López-Nieto J M, Oxidative dyhydrogenation of short chain alkanes on supported vanadium oxide catalysts, *Appl Catal A: Gen*, 157 (1997) 117.
5 Jagtap R, Sakate S & Pardeshi S, Selective N-acetylation with concurrent S-oxidation of o-amino thiol at ambient conditions over Ce doped ZnO composite nanocrystallites, *J Mol Catal*, 450 (2018) 19.
6 Carabineiro S A C, Chen X, Martynyuk O, Bogdanchikova N, Avalos-Borja M, Pestryakov A, Tavares P B, Órfão J J M, Pereira F M R & Luís F J, Gold supported on metal oxides for volatile organic compounds total oxidation, *Catal Today*, 244 (2015) 103.
7 Garcia T, Solsona B & Taylor S H, Naphthalene total oxidation over metal oxide catalysts, *Appl Catal B: Environ*, 66 (2006) 92.
8 Chang R, Zhu L, Jin F, Fan M, Liu J, Jia Q, Tang C & Li Q, Production of bio-based p-xylene via catalytic pyrolysis of biomass over metal oxide-modified HZSM-5 zeolites, *J Chem Technol Biotechnol*, 93 (2018) 3292.
9 Barta K, Warner G R, Beach E S & Anastas P T, Depolymerization of organosolv lignin to aromatic compounds over Cu-doped porous metal oxides, *Green Chem*, 16 (2014) 191.
10 Chouhan A P S & Sarma A K, Modern heterogeneous catalysts for biodiesel production: A comprehensive review, *Renew Sust Energy Rev*, 15 (2011) 4378.

11 Lazar M A, Varghese S & Nair S S, Photocatalytic water treatment by titanium dioxide: Recent updates, *Catalysts*, 2 (2012) 572.

12 Gautam S, Agrawal H, Thakur M, Akbari A, Sharda H, Kaur R & Amini M, Metal oxides and metal organic frameworks for the photocatalytic degradation: A review, *J Environ Chem Eng*, 8 (2020) 103726.

13 Raizada P, Soni V, Kumar A, Singh P, Khan A A P, Asiri A M, Thakur V K & Van-Huy N, Surface defect engineering of metal oxides photocatalyst for energy application and water treatment, *J Mater*, 7 (2021) 388.

14 Khan M M, Adil S F & Al-Mayouf A, Metal oxides as photocatalysts, *J Saudi Chem Soc*, 19 (2015) 462.

15 Noureddine B, Qourzal S, Assabbane A, Ait-Ichou Y, Nounah A, Lachheb H & Houas A, Solar photocatalytic degradation of textile dyes on dynamic pilot plant using supported TiO2, *Arab J Sci Eng*, 35 (2010) 131.

16 Munoz I, Rieradevall J, Torrades F, Peral J & Domènech X, Environmental assessment of different solar driven advanced oxidation processes, *Solar Energy*, 79 (2005) 369.

17 Tijani J O, Fatoba O O, Madzivire G & Petrik L F, A review of combined advanced oxidation technologies for the removal of organic pollutants from water, *Water Air Soil Pollut*, 225 (2014) 1.

18 Bagheri S & Julkapli N M, Mixed-phase $TiO_2$ photocatalysis: Correlation between phase composition and photodecomposition of water pollutants, *Rev Inorg Chem*, 37 (2017) 11.

19 Simonsen M E, Heterogeneous photocatalysis, *Chem Adv Environ Purif Process Water*, Elsevier, (2014) 135.

20 El-Kemary M, El-Shamy H & El-Mehasseb I, Photocatalytic degradation of ciprofloxacin drug in water using ZnO nanoparticles, *J Lumin*, 130 (2010) 2327.

21 Šojić D V, Despotović V N, Abazović N D, Čomor M I & Abramović B F, Photocatalytic degradation of selected herbicides in aqueous suspensions of doped titania under visible light irradiation, *J Hazard Mater*, 179 (2010) 49.

22 Vaya D & Surolia P K, Semiconductor based photocatalytic degradation of pesticides: An overview, *Environ Technol Innov*, 20 (2020) 101128.

23 Viswanathan B, Photocatalytic degradation of dyes: an overview, *Curr Catal*, 7 (2018) 99.

24 Lellis B, Fávaro-Polonio C Z, Pamphile J A & Polonio J C, Effects of textile dyes on health and the environment and bioremediation potential of living organisms, *Biotechnol Res Innov*, 3 (2019) 275.

25 Hassaan M A, El-Nemr A & Hassaan A, Health and environmental impacts of dyes: Mini review, *Am J Environ Sci Eng*, 1 (2017) 64.

26 Sowik J, Miodyńska M, Bajorowicz B, Mikolajczyk A, Lisowski W, Klimczuk T, Kaczor D, Medynska A Z & Malankowska A, Optical and photocatalytic properties of rare earth metal-modified ZnO quantum dots, *Appl Surface Sci*, 464 (2019) 651.

27 Jyothi M S, Nayak V, Reddy K R, Naveen S & Raghu A V, Non-metal (oxygen, sulphur, nitrogen, boron and phosphorus)-doped metal oxide hybrid nanostructures as highly efficient photocatalysts for water treatment and hydrogen generation, In *Nanophotocatalysis and Environmental Applications*, (2019) 83.

28 Kumar R & Dosanjh H S, A mini-review on rare earth metal doped ZnO nanomaterials for photocatalytic remediation of waste water, In *Journal of Physics: Conference Series*, IOP Publishing, 2267 (2022) 012139.

29 Kaldante Y D, Shirsat R N & Chaskar M G, Photocatalytic degradation of Rose Bengal dye over mechanochemically synthesized zinc oxide under visible light irradiation, *Nanosyst: Phys Chem Math*, 12 (2021) 773.

30 Aparna P U, Divya N K & Pradyumnan P P, Structural and dielectric studies of Gd doped ZnO nanocrystals at room temperature, *J Mater Sci Chem Eng*, 4 (2016) 79.

31 Chauhan J, Shrivastav N, Dugaya A & Pandey D, Synthesis and characterization of Ni and Cu doped ZnO, *J Nanomed Nanotechnol*, 1 (2017) 26.

32 Nafees M, Liaqut W, Ali S & Shafique M A, Synthesis of ZnO/Al: ZnO nanomaterial: structural and band gap variation in ZnO nanomaterial by Al doping, *Appl Nanosci*, 3 (2013) 49.

33 Thangeeswari T, Parthipan G & Shanmugan S, Synthesize of gadolinium-doped ZnO nano particles for energy applications by enhance its optoelectronic properties, *Mater Today: Proc*, 34 (2021) 448.

34 Shi-Yong Y, Hong-Jie Z, Ze-Ping P, Li-Ning Sun & Wei-Dong S, Template-free fabrication of hexagonal ZnO microprism with an interior space, *Inorg Chem*, 46 (2007) 8019.

35 Rezapour M & Talebian N, Comparison of structural, optical properties and photocatalytic activity of ZnO with different morphologies: Effect of synthesis methods and reaction media, *Mater Chem Phys*, 129 (2011) 249.

36 Huang M H, Wu Y, Feick H, Tran N, Weber E & Yang P, Catalytic growth of zinc oxide nanowires by vapor transport, *Adv Mater*, 13 (2001) 113.

37 Li W, Wang G, Chen C, Liao J & Li Z, Enhanced visible light photocatalytic activity of ZnO nanowires doped with Mn2+ and Co2+ ions, *Nanomaterials*, 7 (2017) 20.

38 Behnajady M A, Modirshahla N & Hamzavi R, Kinetic study on photocatalytic degradation of CI Acid Yellow 23 by ZnO photocatalyst, *J Hazard Mater*, 133 (2006) 226.

39 Kumar S G & R Kavitha, Lanthanide ions doped ZnO based photocatalysts, *Sep Purif Technol*, 274 (2021) 118853.